Chemical Physics Letters 771 (2021) 138484

Contents lists available at ScienceDirect

Chemical Physics Letters

journal homepage: www.elsevier.com/locate/cplett

Research paper

Elucidation of the structures of aluminate ions during the dissolution of gibbsite in choline and verification of hydrated ion model

Jianwei Guo [a,b,c], Zhihao Shi [a,b], Zhenjie Cui [a,b,c], Zhi Wang [a,b,c,*], Jianwei Cao [a,b], Xuzhong Gong [a,b,c]

[a] Key Laboratory of Green Process and Engineering, National Engineering Laboratory for Hydrometallurgical Cleaner Production Technology, Institute of Process Engineering, Chinese Academy of Sciences, Beijing 100190, China
[b] Innovation Academy for Green Manufacture, Chinese Academy of Sciences, Beijing 100190, China
[c] School of Chemical Engineering, University of Chinese Academy of Sciences, Beijing 100049, China

ARTICLE INFO

Keywords:
Hydrated ion model
Equilibrium solubility
Conductivity
Aluminates structure
Organic alkali

ABSTRACT

The equilibrium solubility of gibbsite in choline was measured and thee quilibrium constant was obtained. Gibbsite was more likely to dissolve in choline compared with NaOH and the dissolution enthalpy was 17.845 kJ/mol. Ion solvation model which can express the equilibrium solubility within the entire alkali concentration range was established and verified by measuring conductivity, solubility parameters. The hydration ion number was obtained 4.83 at 70 °C which was reasonable. The ionic composition of the aluminate solution was studied in choline. With the increase of alkali concentration, $Al(OH)_5^-$ and double oxygen bridged dimer $Al_2O_8H_6^{4-}$ appear and coexist with tetracoordinated $Al(OH)_4^-$.

1. Introduction

Gibbsite is an intermediate compound produced during commercial alumina production. Low decomposition ratio and long decomposition time is the key obstacle in the aluminum production industry and nuclear waste processing [1–4]. The precipitation of gibbsite from caustic aluminate solution is the rate-limiting step in the Bayer process [5,6]. Aluminium hydroxide crystallization in organic base has greatly solved the challenge [7,8]. Dissolution of gibbsite in organic base remains blank which is the key to high efficiency and low cost production.

Enormous works investigated the composition, property, and dynamic dissolution model of in caustic alkali aqueous solution. However, organic alkaline such as tetramethylammonium alkaline (TMAH) and Choline alkaline (ChOH) aqueous was verified to be excellent mediums to control and explore the decomposition process of aluminates because of better solution stability and more mild transformation process [7,8]. The Al-water reaction promoted by TMAH is the most efficient way to activate aluminum with apparent activation energy of 45.92 kJ/mol. The value is much smaller than the value obtained by activating aluminum through inorganic alkali or adulterating of other activation agents. Hence, it is very essential to investigate the composition, properties, and thermodynamic model in the new organic alkali aqueous solution system.

It is consensus that tetrahedral monomer $Al(OH)_4^-$ is the major component of aluminate solution [9,10]. However, as the concentration increases, the hydrated ions dehydrate. The species and population distribution change significantly. Moolenaar [11] speculated the existence of $Al_2O(OH)_6^{2-}$ dimer ions in high concentrated sodium aluminate solution by comparing the liquid-phase with solid-state Raman spectroscopy. In combination with quantum calculation, Liu et al. [12,13] believed that $Al(OH)_4^-$ convert to $Al_2O_6H_4^{2-}$, $Al_4O_{10}H_6^{2-}$ and hexameric 6AlO-OH growth unit of Gibbsite with the increase of concentration. Gale et al. [14] predicted that dimerization to the doubly hydroxyl-bridged species $(OH)_3Al(OH)_2Al(OH)_3^{2-}$ can occur at high concentrated sodium aluminate and that is assisted by the coordination of two or more water molecules. It is interesting to note that the solvation of aluminate results in the variation of original $Al(OH)_4^-$ spatial structure and physical/chemical properties such as thermodynamic barrier [15–19]. The increase of solution concentration promotes the dehydration and polymerization of monomeric $Al(OH)_4^-$. However, the aluminates structure and the transformation pathway in organic system remain ambiguous especially when solvation is under consideration.

* Corresponding author at: Key Laboratory of Green Process and Engineering, National Engineering Laboratory for Hydrometallurgical Cleaner Production Technology, Institute of Process Engineering, Chinese Academy of Sciences, Beijing 100190, China.
E-mail address: zwang@ipe.ac.cn (Z. Wang).

https://doi.org/10.1016/j.cplett.2021.138484
Received 4 December 2020; Received in revised form 26 January 2021; Accepted 23 February 2021
Available online 19 March 2021

A precise equilibrium solubility model brings convenience for practical production. On the one hand, in almost all previous investigations, the solubility in the organic base is usually adopted from the solubility in caustic alkali [20,21], which is rough or irrational [7]. On the other hand, due to the existence of spinodal in the solubility curve, primitive solubility models can only be applied within a specific concentration range. For instance, Misra's empirical formula [21] describe merely the left half curve, it is not appropriate for the right half curve. The insufficiency of solvent water molecules and dispersing medium OH^- ions result in the aforementioned discrepancy. Our recent work [22,23] verified that aluminate monomer exists in the form of $Al(OH)_4^-{\cdot}4H_2O$. Similarly, it has been proved that the enthalpy, a most significant parameter acting on the solubility, decreases when highly hydrated amorphous clusters were formed during calcium carbonate and calcium phosphate nucleation [24–26]. There is a lack of a model that can express the equilibrium solubility within the entire alkali concentration range.

While studying the equilibrium solubility and ionic structure of sodium aluminate solution, some physical and chemical properties of the solution such as electrical conductivity [27] and osmotic coefficients [28] have also been concerned. According to the limit molar conductivity empirical equation of strong electrolyte, Li [29] calculated the migration number of aluminate ions under different Na_2O mass concentrations. It is found that the conductivity of aluminate ion is closely related to solution structure in combination with infrared spectroscopy. Therefore, it is urgent to establish the equilibrium solubility model suitable for the whole concentration range [30–32] based on physicochemical properties especially conductivity.

In this paper, the concentration of aluminum ions in the equilibrium solution was determined by complexometric titration. The gibbsite equilibrium solubility in ChOH was affected by temperature and alkali concentration. An appropriate solvation model was established to express the equilibrium solubility within all concentration range. Thermodynamic data such as reaction equilibrium constant and reaction enthalpy were measured. Finally, the microstructure of organic-aluminate solution was characterized by infrared spectroscopy.

2. Methods and experiments

2.1. Chemicals

$Al(OH)_3$ was supplied by Sinopharm Chemical Reagent CO. LTD (China). The organic choline hydroxide (ChOH) was provided by Jinan Jinhui Chemical Co (China). All reagents were used as received without further purification. High-purity water of 18 MΩ was used.

The reaction temperature was monitored by a temperature sensor within the conductive electrode and kept by a thermostat with precision of ±0.1 °C. The stirring intensity was adjusted by electric mixer. The conductivity is collected by SevenExcellent multi-parameter measuring instrument (China) and transmitted to the computer through LabX direct pH software.

2.2. Preparation of equilibrium solution

A certain amount of choline solution was taken and diluted to 100 mL with deionized water and then placed in 150 mL polyethylene bottles. Required gibbsite was added and the plastic bottles were covered. They were sealed and placed in a constant temperature oscillator (±0.5 °C). The stirring speed was adjusted to 300 rpm, the temperature was set as 30, 50, 70, 90 °C respectively, and the reaction was carried out for 3 days. The solution was filtered after reaction at the reaction temperature, and the concentration of Al_2O_3 and Na_2O in the solution was analyzed by titration of supernatant.

2.3. Titration experiments

The initial alkali concentration was determined by acid-base titration. 0.1% neutral red and methylene blue mixed ethanol solution was used as indicator. At the end of the titration, the indicator color changes from green to blue-violet. The inverse titration method was used to determine the aluminum concentration. Pipette 1 mL solution into the Erlenmeyer flask, then 15 mL 0.01 mol/L EDTA and 80 mL hexamethylenetetramine hydrochloric acid buffer (pH = 5) is added into the solution. Then the pH was adjusted to 3.5 with hydrochloric acid. The mixed solution was boiled for 5 min to complex aluminum ion with EDTA completely. Then sodium hydroxide aqueous and 2 drops of 1% xylenol orange indicator was added to adjust the pH to 5.5. If the solution was yellow, titrate with 0.01 mol/L standard zinc solution until the color turned to lilac. Record the volume of consumed standard zinc solution, the aluminum ion concentration is:

$$C_{Al} = 0.01(15 - V_{Zn}) \tag{1}$$

3. Results and discussions

3.1. Dissolution enthalpy in ChOH

The driving force of crystallization was supplied by supersaturation and it is closely related to equilibrium solubility. For the dissolution reaction of gibbsite, it is consumed that the initial alkali concentration and equilibrium concentration of $Al(OH)_4^-$ are c and × respectively.

$$\begin{aligned} OH^- \quad &+ \quad Al(OH)_3 \rightarrow Al(OH)_4^- \\ t &= 0 \;\; c \;\; 0 \\ t &= \infty \;\; c - x \;\; x \end{aligned} \tag{2}$$

The equilibrium constant K(T) at low concentration is (derivation of the equilibrium constant is shown in supporting information):

$$K(T) = \frac{\gamma_{Al(OH)_4^-} \cdot x}{\gamma_{OH^-} \cdot (c - x)} = \frac{x}{c - x} \tag{3}$$

The equilibrium composition of the solution at 30 °C is shown in Fig. 1a. It can be seen that when the concentration is lower than 0.02 mol/L, the curve is a straight line, which can be regarded as an ideal solution. The equilibrium solubility curves at 50, 70, and 90 °C were measured and showed in Fig. 1b which shows a similar tendency of the curve at 30 °C. The detailed solubility fitting parameters are shown in Table 1.

Mapping lnK(T) to 1/T at different temperatures. The reaction enthalpy can be obtained from the Van't Hoff equation:

$$lnK(T) = -\frac{\Delta_r H_\theta}{R} \cdot \frac{1}{T} + C \tag{4}$$

The obtained reaction enthalpy is $\Delta_r H_\theta = 17.845$ kJ/mol (Fig. 2) and its value is much lower than the value in NaOH reported by Pereira (26.4 kJ/mol) [4] and Li (27.08 kJ/mol) [3]. It indicates that Gibbsite is more likely to dissolve in the organic base. The essence of dissolution of aluminium hydroxide is free OH^- diffuse to the solid surface and then reacts with aluminium hydroxide molecules. Previous work verified that the surface of various aluminium hydroxide polymorphs is highly solvated [33,34]. The OH^- ion must pass through the solvation layer and then react with $Al(OH)_3$. Due to the volume of Choline cation are obviously larger than Na^+. It is deduced that the solvation layer of NaOH system is more compact compared with Choline, the OH^- ion diffuse pass through the solvation layer more easily. Hence, the dissolution enthalpy of ChOH is lower.

3.2. Determination of equilibrium solubility and establishment of hydration ion model

The equilibrium solubility of gibbsite in different choline concen-

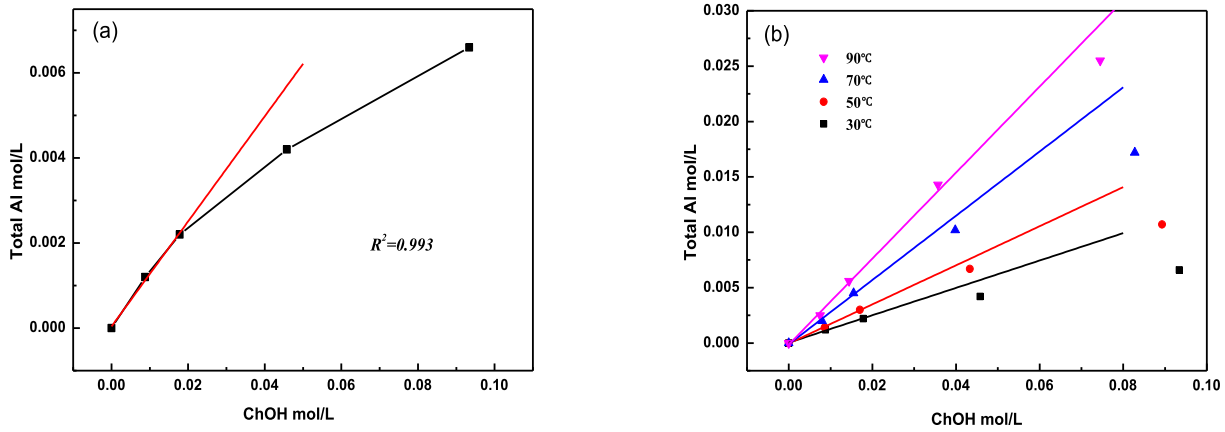

Fig. 1. The equilibrium solubility of Gibbsite at (a) 30 °C and (b) different temperatures.

Table 1
Equilibrium solubility parameters of Gibbsite at different temperature.

T(°C)	$K(T)$	R^2
30	0.1236	0.993
50	0.1764	0.996
70	0.2899	0.986
90	0.3881	0.985

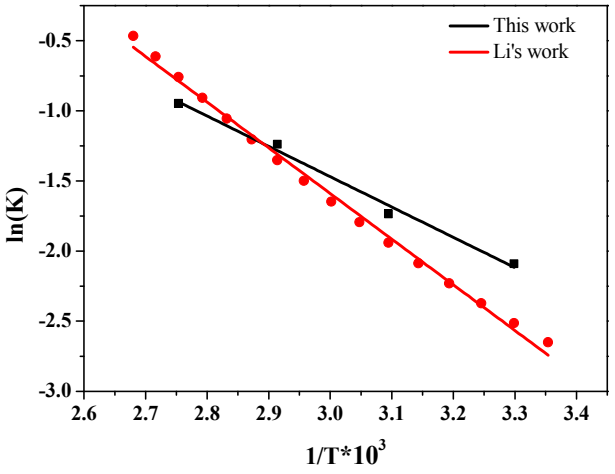

Fig. 2. The Dissolution Enthalpy in ChOH and NaOH.

trations is shown in Fig. 3. The equilibrium solubility of gibbsite increases with temperature and the equilibrium solubility increases first and then decreases with the increase of alkali concentration, which is consistent with the phase diagram of sodium aluminate solution. However, the empirical equation of equilibrium solubility in gibbsite-inorganic base does not fit this system as well, Misra's empirical formula [21] for instance (SI Fig. 1) which describes merely the left half curve. It is speculated that the apparent equilibrium solubility difference between organic and inorganic base system was caused by ignorance of the factor of water concentration. The molecular weight of choline is about 3 times higher than sodium hydroxide (M_{ChOH} = 121.2, M_{NaOH} = 40). The water concentration in NaOH and ChOH can be expressed as follows respectively:

$$\text{in NaOH: } C_{H_2O} = \frac{\rho_{NaOH}}{18} - \frac{40}{18}C_{OH} \quad (5\text{-}1)$$

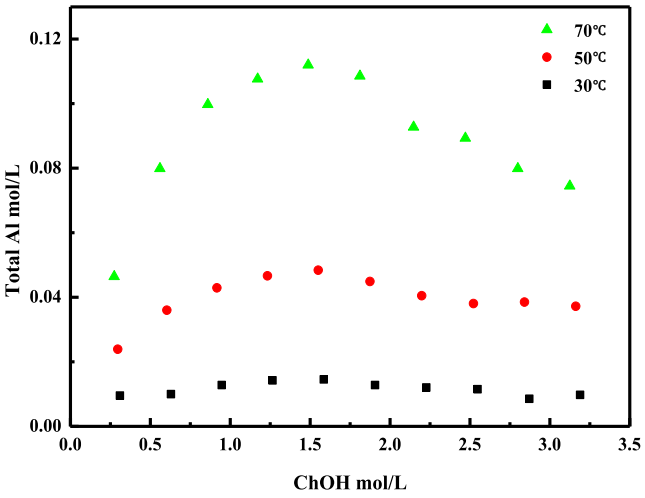

Fig. 3. The equilibrium solubility of Gibbsite in ChOH at various temperatures.

$$\text{in ChOH: } C_{H_2O} = \frac{\rho_{ChOH}}{18} - \frac{121.2}{18}C_{OH} \quad (5\text{-}2)$$

The density of ChOH and NaOH aqueous was measured by weights-volume methods and the water concentration in the two solutions is shown in Fig. 4. It is obvious that at the same alkali concentration, the

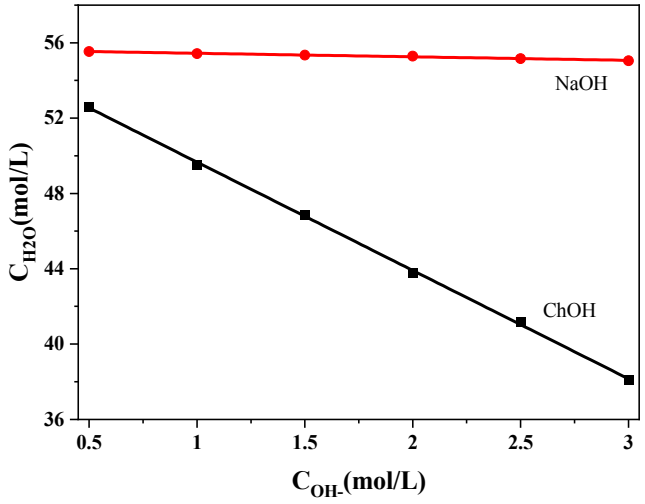

Fig. 4. Water concentration in NaOH and ChOH solution.

mass fraction of choline is much larger which leads to a significant decrease of water concentration. Hence, the curve of the left half is no longer applicable. It can be seen that in the organic alkali solution, the concentration of water decreases with the increase of OH^- concentration, which is higher than that of NaOH. Therefore, the effect of water on the dissolution of gibbsite is more obvious at the same concentration. When the solubility of alumina in NaOH is still in the left half, it may reach the right half in ChOH. At this time, the increase in alkali concentration does not necessarily contribute to the increase of equilibrium solubility.

Water plays a very important role in the dissolution process of gibbsite, water should also be taken into account as reactant. According to the hydration ion model, the reaction process is:

$$Al(OH)_3 + OH^- + nH_2O \rightarrow [Al(OH)_4 \cdot (H_2O)_n]^-$$

The equilibrium constant is:

$$K = \frac{[Al(OH)_4(H_2O)_n]^-}{[OH^-][H_2O]^n} \quad (6)$$

Hence:

$$[Al] = K(T) \cdot [OH^-][H_2O]^n \quad (7)$$

Take water into consideration, the concentration of aluminate is:

$$C_{Al} = K(T) C_{OH^-} \left(\frac{\rho_{ChOH}}{18} - \frac{121.2}{18} C_{OH^-} \right)^n \quad (8)$$

Assume that the number of hydrated ions n is constant within a certain concentration range. Eq. (8) was used to fit the equilibrium solubility at different temperatures. The fitting curves and the parameters of each fitting equation are shown in Table 2, Fig. 5, and SI Fig. 2.

The fitted results show that the n value is between 5.12 and 5.65. The best result of the fitted solubility curve is at 70 °C and the hydrated water number n of $Al(OH)_4^-$ is 5.50. The n value is influenced by concentration and temperature range. Side reaction leads to the variation of n value. Nevertheless, the result is in consistent with our previous work which proved that the water number is between 4 and 8 [23]. Besides, the fitting result of the equilibrium constant increases with the increase of temperature, which is consistent with the facts, indicating that the model is rational.

3.3. Verification of the hydrated ion model

The total aluminium concentration increase first and then decrease with the increase of choline concentration. This may be caused by the competitive relationship between OH^- and H_2O. In inorganic alkali solution, the influence of the number of water molecules is small with the increment of alkali concentration. The contribution of the increase in OH^- to the dissolution reaction is non-negligible. In ChOH solution, the effect of water concentration is more significant. The decrease of water concentration leads to the reduction of total aluminium concentration ultimately.

On the one hand, water participates in the formation of aluminate anion. On the other hand, it actives OH^-. Therefore, it is assumed that OH^- must combine with water before participating in the reaction. In other words, the process of dissolving gibbsite is divided into two steps.

Table 2
The equilibrium solubility fitting parameters of Gibbsite at different temperature.

T(°C)	K(T)	n	R^2
30	$3.40*10^{-12}$	5.65	0.60
50	$9.03*10^{-11}$	5.12	0.775
70	$4.80*10^{-11}$	5.50	0.960

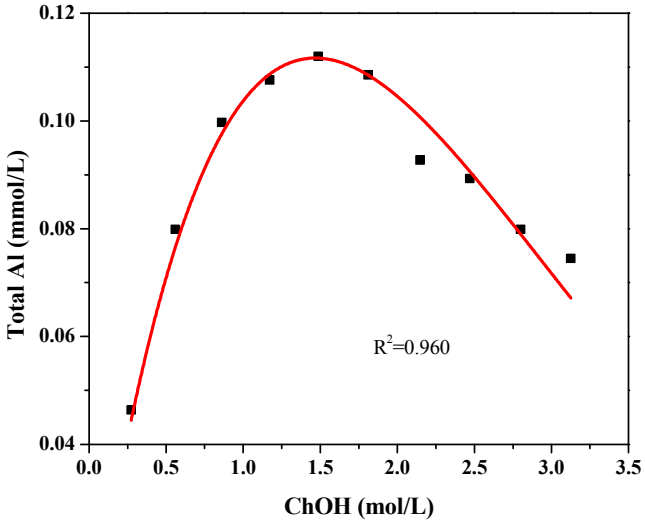

Fig. 5. The fitting of equilibrium solubility curve of Gibbsite in ChOH at 70 °C.

$$OH^- + nH_2O \rightarrow OH^- \cdot nH_2O$$
$$Al(OH)_3 + OH^- \cdot nH_2O \rightarrow [Al(OH)_4 \cdot (H_2O)_n]^-$$

The equilibrium constants for each step are:

$$K_1 = \frac{[OH^- \cdot nH_2O]}{[OH^-][H_2O]^n} \quad (9)$$

$$K_2 = \frac{[Al(OH)_4 \cdot (H_2O)_n]^-}{[OH^- \cdot nH_2O]} \quad (10)$$

The total equilibrium constant is:

$$K_{12} = K_1 \cdot K_2 = \frac{[Al(OH)_4(H_2O)_n]^-}{[OH^-][H_2O]^n} \quad (11)$$

$$\text{Hence : } [Al] = K(T) \cdot [OH^-][H_2O]^n \quad (12)$$

$$[OH^- \cdot nH_2O] = K_1 \cdot [OH^-][H_2O]^n \quad (13)$$

The conductivity of the aqueous aluminate choline solution at different temperatures was measured and shown in Fig. 6. Since the equilibrium constants K_1, K_2, K(T) are both a function of temperature, they are independent of the reactant concentration. The tendency of the equilibrium solubility curve and the reacted OH^- concentration curve are similar. The conductivity curve of the choline solution is exactly this

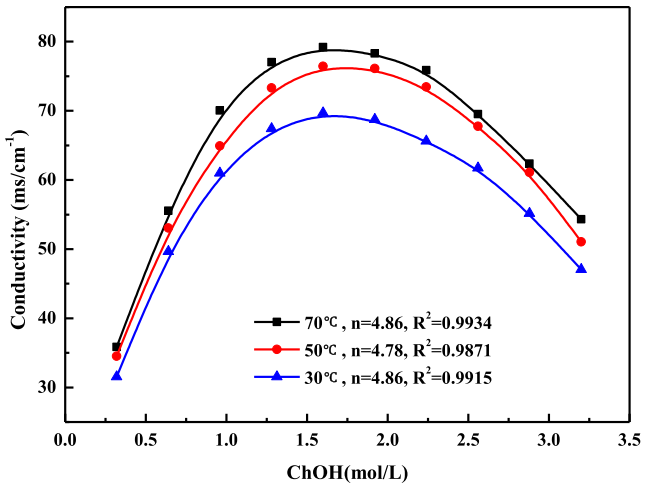

Fig. 6. The conductivity curve of Gibbsite in ChOH at different temperatures.

trend, so it is speculated that in aluminate choline solution, this part of the free moving OH^- that can transport electrons participates in the dissolution reaction of gibbsite [35]. The conductivity curve at 70 °C was fitted as:

$$\sigma = 3.95*10^{-7}\cdot C_{OH}(\frac{\rho_{ChOH}}{18} - \frac{121.2}{18}C_{OH})^{4.83} \quad (14)$$

The equation of the hydration ion model fits the conductivity curve well, which confirms the above conjecture. The water coordination number of the hydrated $Al(OH)_4^-$ is 4.83 which is very close to the result obtained from the solubility curve. We can conclude that water acts as reactant and participates in the dissolution process of gibbsite. Compared with the activity coefficient calculated from the Pitzer model, the hydrated ion model is more concise and convenient.

3.4. Microstructure analysis of organic aluminates based on IR spectrum

The IR spectrums of different organic aluminate solution were depicted in Fig. 7. The infrared absorption of aluminate is mainly below 1000 cm^{-1} and is divided into three zones. 500~750 cm^{-1} is the stretching vibration range of the Al—O bond, and 750~900 cm^{-1} is the vibration of Al—O in AlO_4 unit. 937~980 cm^{-1} is the vibration of the Al—OH bond. It can be seen that 954, 880, 863 cm^{-1} absorption peaks appear in all alkalinity, and they are corresponding to Al of Al—OH stretching and Al—O bond in AlO_4 unit. Therefore, $Al(OH)_4^-$ present in different concentrations of solution. Li and Ding [20] contribute the peaks at 720 cm^{-1} to the stretching vibration of Al—O in tetrahedral Al $(OH)_4^-$ in inorganic sodium aluminate. Watling [36] contributes the shoulder peak at 650 cm^{-1} to AlO_6. When the concentration of alkali range from 0.9 to 2.1 mol/L, peaks that locate at 705 cm^{-1} and 670 cm^{-1} exist. However, when the concentration exceeds 2.1 mol/L and increases to 2.7 mol/L it disappeared. The peak at 705 cm^{-1} is red shifted from the peak at 720 cm^{-1} which indicates that the energy of Al—O bond decrease. The peak at 670 cm^{-1} was blue shifted from 620 cm^{-1} which indicates that the energy of Al—O bond increase. According to the electrostatic bond strength formula:

$$S = \frac{Z}{u} \quad (15)$$

where S is the ionic bond strength, Z is the cationic charge number, and u is the coordination number.

$S_{Al\text{-}O}$ equal to 3/4 and 1/2 in four coordinated and six coordinated aluminate which demonstrates that the bond energy of Al—O in four coordinated is higher than six coordinated aluminates. Hence, it is speculated that the peaks that locate at 705 cm^{-1} and 670 cm^{-1} contribute to the Al—O bond in aluminate which is weaker than four-coordinate and stronger than six-coordinate. In addition, it is generally accepted that the coordination number of Al—O changes from original four coordinated monomers in solution to terminal six coordinated in aluminium hydroxide crystal during the crystallization. Thus it is reasonable to assume that five coordinated aluminate exists in the solution despite few abundance. For the solution with 2.7 mol/L alkali concentration, there is a clear peak at 563 cm^{-1}, indicating the presence of polymerized aluminum ions at this concentration.

In summary, in low organic aluminate concentration, only tetragonal monomer $Al(OH)_4^-$ exists, while in the medium concentration (0.9~2.1 mol/L) organic aluminate solution, tetragonal $Al(OH)_4^-$ and pentatonic $Al(OH)_5^-$ exist, respectively. In higher concentrations of organic aluminates, $Al(OH)_4^-$ and dimeric $[(HO)_3\text{-}Al\text{-}O_2\text{-}Al(OH)_3]^{4-}$, the characteristic peak position are shown in Table 3 and the structures of these molecules are shown in Fig. 8.

4. Conclusions

The equilibrium solubility of gibbsite in choline was measured, and the reaction equilibrium constant at each temperature was obtained,

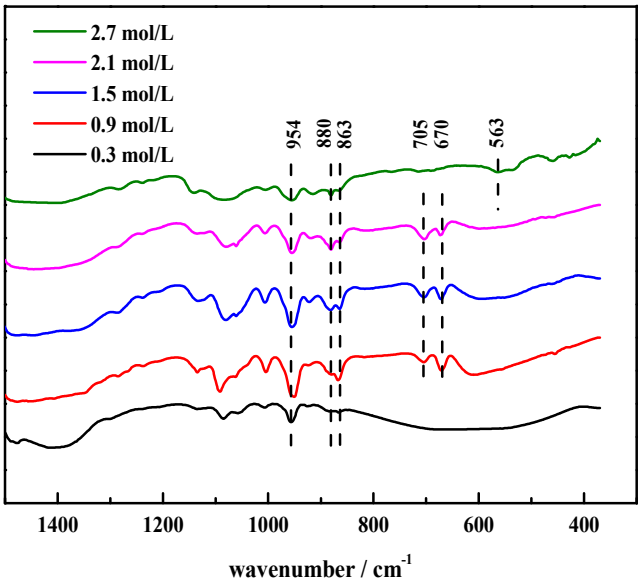

Fig. 7. IR spectra of equilibrium solution with different alkali concentration.

Table 3
IR of organic aluminates.

Alkali concentration (mol/L)	Wavelength (cm^{-1})	Components
0.3	954, 880, 863	$Al(OH)_4^-$
0.9	954, 880, 863, 705, 670	$Al(OH)_4^-$, $Al(OH)_5^-$
1.5	954, 880, 863, 705, 670	$Al(OH)_4^-$, $Al(OH)_5^-$
2.1	954, 880, 863, 705, 670	$Al(OH)_4^-$, $Al(OH)_5^-$
2.7	954, 880, 863, 563	$Al(OH)_4^-$, $Al_2O_8H_6^{4-}$

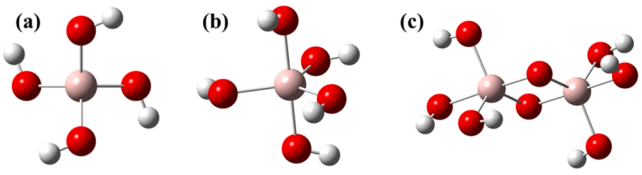

Fig. 8. The structures of alumiantes, (a) $Al(OH)_4^-$, (b) $Al(OH)_5^-$, (c) $Al_2O_8H_6^{4-}$.

which was extremely close to the value reported in the literature. The calculated dissolution enthalpy was 17.845 kJ/mol which was much lower than the value in NaOH. It indicated that Gibbsite is more likely to dissolve in organic base. The hydrated ion model was established and verified by measuring the conductivity, equilibrium solubility, and other parameters which indicated that water molecules play important role in organic alkali solution. The hydration water numbers obtained by the two models were 5.50 and 4.83 respectively which is in consistent with our previous simulated work. This model can express the equilibrium solubility and conductivity within the entire alkali concentration range. The ionic composition of the aluminate solution was studied in the choline system. It was found that the only form of aluminate at low concentration is tetracoordinated monomer $Al(OH)_4^-$, in the high organic aluminate concentration, $Al(OH)_4^-$ and double oxygen bridged dimeric $Al_2O_8H_6^{4-}$ coexist. However, at moderate concentrations (0.9~2.1 mol/L), penta-coordinated $Al(OH)_5^-$ coexist which may act as intermediate in the process of aluminate polymerization. This research on the composition of organic aluminate equilibrium solution and ion solvation can help better enhancing the decomposition depth and improve the precipitation ratio.

Associated content

The detailed derivation of equilibrium constant and the equilibrium solubility curve of Gibbsite in ChOH at 30 and 50 °C are displayed in supporting information.

Declaration of Competing Interest

The authors declare that they have no known competing financial interests or personal relationships that could have appeared to influence the work reported in this paper.

Acknowledgments

This work was partially funded by the National Key R&D Program of China (2018YFC1901801) and the National Natural Science Foundation of China (51974286).

Appendix A. Supplementary material

Supplementary data to this article can be found online at https://doi.org/10.1016/j.cplett.2021.138484.

References

[1] P. Bénézeth, D.A. Palmer, D.J. Wesolowski, Dissolution/precipitation kinetics of boehmite and gibbsite: Application of a pH-relaxation technique to study near-equilibrium rates, Geochim. Cosmochim. Ac. 72 (2008) 2429–2453.
[2] H. Grenman, T. Salmi, D.Y. Murzin, J. Addai-Mensah, The dissolution kinetics of gibbsite in sodium hydroxide at ambient pressure, Ind. Eng. Chem. Res. 49 (2010) 2600–2607.
[3] X.B. Li, L. Yan, Q.S. Zhou, G.H. Liu, Z.H. Peng, Thermodynamic model for equilibrium solubility of gibbsite in concentrated NaOH solutions, T Nonferr. Metal. Soc. 22 (2012) 447–455.
[4] J.A.M. Pereira, M. Schwaab, E. Dell'Oro, J.C. Pinto, J.L.F. Monteiro, C. A. Henriques, The kinetics of gibbsite dissolution in NaOH, Hydrometallurgy 96 (2009) 6–13.
[5] I. Anich, T. Bagshaw, N. Margolis, M. Skillingberg, The alumina industry roadmap, essential readings in light metals: alumina and bauxite. 1 (2013) 94–99.
[6] X. Li, D. Wang, Q. Zhou, G. Liu, Z. Peng, Concentration variation of aluminate ions during the seeded precipitation process of gibbsite from sodium aluminate solution, Hydrometallurgy 106 (2011) 93–98.
[7] H.Q. Wang, Z. Wang, L. Liu, X.Z. Gong, M. Wang, Alumina hydrate polymorphism control in Al-water reaction crystallization by seeding to change the metastable zone width, Cryst. Growth Des. 16 (2016) 1056–1062.
[8] H.Q. Wang, Z. Wang, Z.H. Shi, X.Z. Gong, J.W. Cao, M.Y. Wang, Facile hydrogen production from Al-water reaction promoted by choline hydroxide, Energy. 131 (2017) 98–105.
[9] L.A. Carreira, V.A. Maroni, J.W. Swaine, R.C. Plumb, Raman and infrared spectra and structures of the aluminate ions, J. Chem. Phys. 45 (1966) 2216–2220.
[10] P. Sipos, G. Hefter, P.M. May, ^{27}Al NMR and Raman spectroscopic studies of alkaline aluminate solutions with extremely high caustic content - Does the octahedral species $Al(OH)_6^{3-}$ exist in solution? Talanta 70 (2006) 761–765.
[11] R.J. Moolenaar, J.C. Evans, L.D. McKeever, Structure of the aluminate ion in solutions at high pH, J. Phys. Chem. 74 (1970) 3629–3636.
[12] W. Liu, Y.L. Huang, Z.L. Yin, Z.Y. Ding, Investigation on the decomposition process of sodium aluminate solution by spectroscopic and theoretical calculation, J. Mol. Liq. 261 (2018) 115–122.
[13] W. Liu, Z. Yin, Y. Huang, Z. Ding, Study on the structure and generation mechanism of intermediate (6AlO–OH) in decomposition process of sodium aluminate solutions, TMS Annual Meeting & Exhibition. (2018).
[14] J.D. Gale, A.L. Rohl, H.R. Watling, G.M. Parkinson, Theoretical investigation of the nature of aluminum-containing species present in alkaline solution, J. Phys. Chem. B 102 (1998) 10372–10382.
[15] J.D. Kubicki, D. Sykes, S.E. Apitz, Ab Initio Calculation of Aqueous Aluminum and Aluminum−Carboxylate Complex Energetics and ^{27}Al NMR Chemical Shifts, J. Phys. Chem. A 103 (1999) 903–915.
[16] B.M. Lu, X.Y. Jin, J. Tang, S.P. Bi, DFT studies of Al-O Raman vibrational frequencies for aquated aluminium species, J. Mol. Struct. 982 (2010) 9–15.
[17] T. Radnai, P.M. May, G.T. Hefter, P. Sipos, Structure of aqueous sodium aluminate solutions: A solution X-ray diffraction study, J. Phys. Chem. A 102 (1998) 7841–7850.
[18] A.J. Sillanpaa, J.T. Paivarinta, M.J. Hotokka, J.B. Rosenholm, K.E. Laasonen, A computational study of aluminum hydroxide solvation, J. Phys. Chem. A 105 (2001) 10111–10122.
[19] J.A. Tossell, Theoretical studies on aluminate and sodium aluminate species in models for aqueous solution: $Al(OH)_3$, $Al(OH)_4$, and $NaAl(OH)_4$, Am. Mineral. 84 (1999) 1641–1649.
[20] J. Li, J. Addai-Mensah, A. Thilagam, A.R. Gerson, Growth mechanisms and kinetics of gibbsite crystallization: experimental and quantum chemical study, Cryst. Growth Des. 12 (2012) 3096–3103.
[21] C. Misra, E.T. White, Crystallisation of bayer aluminium trihydroxide, J. Cryst. Growth 8 (1971) 172–178.
[22] J. Guo, S. Liu, Z. Wang, J.W. Cao, D. Wang, Polymerization of aluminate monomer in its initial nucleation stage of organic alkali solution revealed by ReaxFF molecular dynamics simulation, Chem. Phys. Lett. 739 (2020) 136979.
[23] J. Guo, Z. Wang, J. Cao, X. Gong, Structures of solvated tetramethylammonium aluminate species and its transformation mechanism by DFT and Raman spectra, J. Mol. Struct. 1199 (2020) 126791.
[24] A. Dey, P.H. Bomans, F.A. Muller, J. Will, P.M. Frederik, G. de With, N. A. Sommerdijk, The role of prenucleation clusters in surface-induced calcium phosphate crystallization, Nat. Mater. 9 (2010) 1010–1014.
[25] M. Farhadi-Khouzani, D.M. Chevrier, P. Zhang, N. Hedin, D. Gebauer, Water as the key to proto-aragonite amorphous $CaCO_3$, Angew. Chem. Int. Ed. Engl. 55 (2016) 8117–8120.
[26] P. Raiteri, J.D. Gale, Water is the key to nonclassical nucleation of amorphous calcium carbonate, J. Am. Chem. Soc. 132 (2010) 17623–17634.
[27] J. Li, Z.L. Yin, Z.Y. Ding, W. Liu, T.R. Wei, Q.Y. Chen, W.Y. Zhang, Homogeneous nucleation of $Al(OH)_3$ crystals from supersaturated sodium aluminate solution investigated by in situ conductivity, Hydrometallurgy 163 (2016) 77–82.
[28] J. Zhou, Q.Y. Chen, J. Li, Z.L. Yin, X. Zhou, P.M. Zhang, Isopiestic measurement of the osmotic and activity coefficients for the NaOH-$NaAl(OH)_4$–H_2O system at 313.2 K, Geochim Cosmochim Ac. 67 (2003) 3459–3472.
[29] X. Li, D. Wang, S. Liang, G. Liu, Z. Peng, Q. Zhou, Relationship between electric conductivity and ion structure of sodium aluminate solution, Chem J Chinese U. 31 (2010) 1651–1655.
[30] J. Anwar, D. Zahn, Uncovering molecular processes in crystal nucleation and growth by using molecular simulation, Angew. Chem. Int. Ed. Engl. 50 (2011) 1996–2013.
[31] P. Sipos, The structure of Al(III) in strongly alkaline aluminate solutions-A review, J. Mol. Liq. 146 (2009) 1–14.
[32] D. Zahn, Thermodynamics and kinetics of prenucleation clusters, classical and non-classical nucleation, Chemphyschem. 16 (2015) 2069–2075.
[33] S. Lectez, J. Roques, M. Salanne, E. Simoni, Car-Parrinello molecular dynamics study of the uranyl behaviour at the gibbsite/water interface, J. Chem. Phys. 137 (2012) 154705.
[34] Z. Shen, E.S. Ilton, M.P. Prange, S.N. Kerisit, Molecular dynamics simulations of the interfacial region between boehmite and gibbsite basal surfaces and high ionic strength aqueous solutions, J. Phys. Chem. C 121 (2017) 13692–13700.
[35] M. Yamada, I. Honma, Anhydrous proton conductive membrane consisting of chitosan, Electrochim. Acta 50 (2005) 2837–2841.
[36] H.R. Watling, P.M. Sipos, L. Byrne, G.T. Hefter, P.M. May, Raman, IR, and ^{27}Al-MAS-NMR spectroscopic studies of sodium (hydroxy)aluminates, Appl. Spectrosc. 53 (1999) 415–422.